Journal of Materials Chemistry A

Energy harvesting and electricity production through dissolved carbon dioxide by connecting two form-stable phase change materials

Journal:	*Journal of Materials Chemistry A*
Manuscript ID	TA-ART-11-2023-006766.R1
Article Type:	Paper
Date Submitted by the Author:	04-Feb-2024
Complete List of Authors:	Yu, Chengbin; Louisiana State University and A&M College, Mechanical & Industrial Engineering; Konlan, John; Louisiana State University, Department of Mechanical & Industrial Engineering Li, Guoqiang; Louisiana State University, Mechanical Engineering

Energy harvesting and electricity production through dissolved carbon dioxide by connecting two form-stable phase change materials

Chengbin Yu[a], John Konlan[a], Guoqiang Li[a,b,*]

[a] *Department of Mechanical and Industrial Engineering, Louisiana State University, Baton Rouge, LA 70803, United States of America*

[b] *Department of Mechanical Engineering, Southern University and A &M College, Baton Rouge, LA 70813, United States of America*

***Corresponding author:** lguoqi1@lsu.edu

Abstract

Herein, we report a new solar energy harvesting approach by connecting two form-stable phase change materials under moist environment dissolved with carbon dioxide (CO_2). Recently, a smart and creative energy harvesting concept has emerged by using form-stable phase change material (PCM) composites without any thermoelectric device. In that approach, the two form-stable PCM composites must have different electrical resistivity and phase transition temperatures based on the Seebeck effect. In this study, there is no need to make the PCM composite an electrical conductor. Instead, we propose to use different relative humidity on the surfaces of the two connected PCM composites and use dissolved carbon dioxide as the moving ions to produce electricity. To this purpose, we synthesized, and 3D printed a hydrophilic shape memory vitrimer (SMV) container as the supporting material. By infiltrating two types of PCMs into the SMV supporting container, two types of PCM composites were obtained. By changing the surface moisture content and the concentration of dissolved CO_2, PCM composites with different electrical resistivities were realized. Comprehensive characterizations were conducted on the synthesized SMV, PCMs, and PCM composites. The effect of the relative humidity and CO_2 concentrations on the electrical energy outputs were investigated. For groups or assembly were further investigated. It was found that the assembly made of SMV supported 1-tetredecanol with 70% relative humidity and SMV supported polyethylene glycol with 90% relative humidity under 700 ppm and 1200 ppm CO_2

concentrations preformed the best. The voltage and current outputs were about 2.73 mV and 500 nA under light-on/off process, respectively. Numerical simulation was also conducted, which largely confirmed the experimental results. This study shows that greenhouse gas can be effectively employed to harvest energy. It is believed that this study provided new opportunities for clean energy harvesting.

Keywords: carbon dioxide, vitrimer, phase change material, energy harvesting, relative humidity

1. Introduction

Nowadays, energy harvesting is one of the most important issues due to depletion of fossil fuels and the climate change due to greenhouse effect. The daily consumption of fossil fuel leads to environmental pollution and climate change. Replacement of fossil fuel by clean and renewable energy is indispensable to reduce both the energy crisis and environmental destruction[1, 2]. To achieve the objective, clean energy harvesting is a current mission in both academic and industrial research. Solar energy is an abundant clean energy source that can contribute to preventing the energy crisis effectively[3, 4]. In theory, the amount of solar energy reaching the Earth for one hour is equal to one year's energy consumption in the world[5]. Therefore, utilization of solar energy is quite important to provide adequate power sources for energy consumption[6, 7]. Harnessing sunlight to generate electrical energy has been done by solar cells[8, 9]. It is related to the solar photovoltaic (PV) system which can convert sunlight into usable electricity directly[10, 11]. Moreover, solar energy can be utilized for solar heating and cooling applications to generate electrical energy according to the Seebeck effect[12, 13]. The solar energy device results in solar-to-electrical energy harvesting under the existence of temperature difference between the two sides of the device[14, 15]. While solar energy devices, especially those based on Seebeck effect, show numerous advantages, they must accumulate sunlight and store it as thermal energy for a long time. Increasing the duration of solar energy harvesting requires a suitable substance with a high thermal energy storage (TES) capacity. Phase change material (PCM) is recognized as such a material.

A PCM exhibits a high heat of fusion which can absorb and release a large amount of thermal energy during the phase transition process due to the high latent heat and thermal density[16, 17]. When a PCM undergoes solid-liquid phase change, the intermolecular structures are disrupted, which demands a lot of energy to break the intermolecular bonds[18, 19]. Thus, the PCM shows a nearly isothermal state when it changes from solid to liquid and stores a plenty of thermal

energy effectively[20, 21]. Similar to the liquid to solid crystallization process, intermolecular bonds form when the stored energy starts to release. Therefore, the reversible phase change can produce a stable temperature difference for harvesting thermoelectric energy [22, 23]. Because of high latent heat, appropriate phase transition temperature, and excellent chemical stability, solid-liquid PCMs have been extensively utilized for numerous applications through high latent heat thermal energy storage (LHTES)[24, 25]. However, the leakage problem during solid to liquid phase change restricts the widespread utilization of pure PCMs since it is difficult to prevent the initial solid state from leaking during the melting process[26, 27]. It requires some kinds of supporting materials to prevent the leakage. To this end, microencapsulation and vacuum impregnation methods have been adopted to fabricate form-stable PCM composites.

Recently, polyaniline (PANI) and poly(methyl methacrylate) (PMMA) have been used as supporting materials to fabricate microencapsulated PCM composites[28, 29]. This type of encapsulated microsphere structure can maintain the PCM without any leakage during the phase transition process. For the sake of increasing the weight fraction of the pure PCM, porous supporting materials have been selected and pure PCM have been infiltrated into the pore volume to obtain a form-stable PCM composite[30, 31]. Considering that carbon based material can absorb sunlight efficiently, graphene aerogel supported PCM composite has also been utilized for constructing a solar-to-electrical power generator and produced stable and continuous electrical energy output during the light-on/-off process[32, 33]. In addition, two types of PCM composites with different phase transition temperatures have been connected to each side of a power generator to generate electrical energy during the heating and cooling processes[34, 35]. The working condition of this model is close to practical applications, which is possible to generate electrical energy merely under the change of external temperatures. Although excellent studies have been reported recently by connecting PCM composites with

energy harvesting devices to produce electrical energy, it remains a limitation for further utilization because the energy harvesting devices are costly.

Herein, we propose to eliminate the energy harvesting devices by directly connecting two types of PCM composites with different electrical conductivities and different phase change temperatures. It works under the Seebeck effect. In particular, we propose to produce the different electrical conductivities by changing the surface humidity of the PCM composites with different concentrations of dissolved carbon dioxide (CO_2).

Unlike previous studies, in this study, we propose to use 3D printed hydrophilic shape memory vitrimer (SMV) or vitrimer for short as the supporting material to prepare form-stable PCM composites. One reason of using SMV to manufacture the supporting container is that under cyclic thermal loading, fatigue failure may occur in the container of the form-stable PCM composites. The cracks, if not healed, will lead to leaking of the PCM. As a result, the energy harvesting assembly will stop working. Furthermore, at the end of the service life, one may want to recycle the container and the PCM to make the system sustainable. SMVs, as chemically cross-linked thermoset polymers, have outstanding mechanical properties, shape memory effect, self-healing capability, and recyclability[36, 37]. Particularly, combination of shape memory effect and intrinsic self-healing capability can help heal wider opened cracks per the biomimetic close-then-heal (CTH) strategy[38-40]. Although most SMVs exhibit low electrical conductivity, it can be increased rapidly under the moisture environment with high concentrations of carbon dioxide (CO_2)[41], if the SMVs are hydrophilic. Therefore, by simply changing the humidity and the concentration of carbon dioxide on the surface of the hydrophilic SMV supporting material, different electrical conductivities can be obtained. Coupled with the different phase transition temperatures by infiltrating different PCMs, the form-stable PCM composites satisfy the requirement for different electrical conductivities and different phase

transition temperatures. As a result, we hypothesize that electricity can be generated by directly connecting the two PCM composites based on the Seebeck effect.

This idea can be further explained as follows. It has been known that ions in aqueous solution can move from the hot side to the cold side in a medium under the existence of temperature gradient[42]. The ion diffusion ability at the hot side is higher than that at the cold side. The ion movements cause an ion concentration gradient, which produces a potential difference. Therefore, we propose this new idea of obtaining electrical energy by merely using SMV supported two types of PCM composites. Although the dissolving ability of CO_2 is decreased at higher temperatures, both ionization of carbonic acid and ion diffusivity are increased rapidly to speed up the ion movements from the hot side to the cold side. The increase in ion concentration at the cold side promotes the generation of carbonic acid and recombine into CO_2. In a word, the CO_2 enters the hot side, decomposes into ions, moves to the cold side, and recombines into CO_2. Therefore, the greenhouse gas is only used as a medium to produce electricity. The idea does not reduce the emission of greenhouse gas, nor does it increase the greenhouse gas emission. The working principle is further illustrated in **Fig. S1** in the Supplementary Materials.

To produce continuous electricity output, we will use light-on and light-off cycles to maintain a constant temperature gradient between the two SMV-supported PCM composites. The reason is that during the light-on process, both the PCMs change from solid to liquid, absorbing a large amount of heat, but almost keeping the temperature at their corresponding phase transition temperature, thus maintaining a constant thermal gradient, which is one critical requirement for the Seebeck effect. To keep continuous electricity output, a light-off process must follow. During light-off, the two PCMs change from liquid to solid, which releases heat, but almost maintains a constant thermal gradient, again, satisfying the requirement for Seebeck effect. This light-on/-off process completes one cycle. The subsequent cycles will repeat the

first cycle, i.e., a light-on branch, followed by a light-off branch. As a result, continuous and constant temperature gradient will be maintained, leading to continuous electricity production.

In this study, polyethylene glycol (PEG) and 1-tetradecanol (1-TD) are utilized as two types of pure PCMs. The SMV container, which is a rectangular hollow box, is obtained by 3D printing using digital light processing (DLP) type of 3D printer. The two types of PCM composites are then connected with each other and water is sprayed on their surfaces. With different concentrations of carbon dioxide dissolved in the water, which is provided from a CO_2 storage tank, different electrical conductivities between the two sides of the PCM composites can be created, as shown in **Fig. 1**. In the following, we will report the preparation and test results of the new energy harvesting device.

2. Results and discussions

2.1 Morphologies of the synthesized shape memory vitrimer

Fig. S5a and **S5b** show the FTIR peaks of diphenyl carbonate and di(trimethylolpropane) which were utilized as monomers to synthesize the SMV. The C=O peak of the diphenyl appears at 1750 cm^{-1}, and the aromatic structure is close to 3000 cm^{-1}. The C-O peak of di(trimethylolpropane) is detected at 1000 – 1150 cm^{-1}, which indicates the intrinsic structure before the synthesizing process. The tris(2-aminoethylamine) (TREN) result is shown in **Fig. S5c** and the initial Tris[2-(acryloyloxy)ethyl] isocyanurate (TAI) chemical structure is shown in **Fig. 2a**. There are representative peaks of functional groups such as amide, C=O, and C=C that would be crosslinked to a network structure. The TAI only 3D printed pre-vitrimer result is shown in **Fig. S5d**. The two monomers synthesized TAI pre-polymer exhibited different absorption peak intensities, as shown in **Fig. S5e**. After 3D printing, the peak of the final SMV is presented in **Fig. 2b.** The –CH peak intensity is increased during the curing process. It indicates that the diphenyl carbonate and di(trimethylolpropane) synthesized TAI pre-polymer is polymerized into a crosslinked SMV structure. To verify the chemical stability at different

temperatures, **Fig. S5f** shows the FTIR result and there is no chemical reaction from 25 °C to 80 °C. To further demonstrate the synthesis of the SMV by the two monomers, the XPS measurement result is provided. **Fig. S6a** and **S6b** show the results of diphenyl carbonate while **Fig. S6c** and **S6d** are the results of di(trimethylolpropane). After crosslinking these two monomers, the structure is changed, as shown in **Fig. S7**. The N1s peak in **Fig. S7c** indicates that the diphenyl carbonate and di(trimethylolpropane) are crosslinked by TREN effectively. The results of the final 3D printed SMV are presented in **Fig. S8**. All generated functional groups appear in C1s and N1s peaks. In addition, the atomic spectrum of the final SMV is shown in **Fig. S8d** and nitrogen is increased significantly compared with the pre-polymer as shown in **Fig. S7d**. The fabricated SMV exhibits an amorphous structure which is confirmed by the results of Raman peaks as shown in **Fig. S9**. To compare with TAI only 3D printed pre-polymer and the synthesized SMV, **Fig. 2c** shows the TGA results and the characteristics are listed in **Table 1**. It is observed that the synthesized final SMV exhibits better thermal stability than the pre-vitrimer. The stress-strain behaviors are shown in **Fig. S10a**. The tensile strength of the SMV is close to 10.0 MPa while the pre-vitrimer merely stops at 4.8 MPa. Both the TGA and stress-strain results demonstrate that the synthesized SMV has excellent thermal and mechanical properties and is suitable for being utilized as a supporting material to fabricate the form-stable PCM composite.

Fig. 2d shows the contact angle measurement. The synthesized SMV is hydrophilic due to the incorporation of hydrogen functional groups. It can be concluded that the final SMV can easily absorb moisture and dissolve CO_2 from the environment. The surface structure of the SMV was obtained by SEM images, as shown in **Fig. S10b**. The SMV shows a flat surface structure while the 1-TD and PEG contain a lot of wrinkles as presented in **Fig. S10c** and **S10d**.

The result of electrical resistivity under the increase in external relative humidity (RH) is shown in **Fig. 2e**. It is seen that the electrical resistance of the SMV decreases rapidly at RH

70% (the initial RH in the air is 40%). Furthermore, the electrical resistivity of the SMV can be decreased further with the increase in CO_2 concentration (the initial CO_2 concentration in the air is 400 ppm), as shown in **Fig. 2f**. The electrical resistivity of the SMV is decreased from 4.16 kΩ at 40% RH to 1.27 kΩ at RH 70%. At RH 80%, the electrical resistivity is changed from 3.32 kΩ to 1.06 kΩ, while it is changed from 2.57 kΩ to 0.92 kΩ under the RH 90% condition. It is easy to confirm that the electrical resistivity is difficult to decrease with the increase in temperature or CO_2 concentration at the initial RH of 40%, as shown in **Fig. 3a, 3b, and 3c.** One of the key points is that the CO_2 dissolving ability decreases with the increase in external temperature as indicated in **Fig. 3d**[43]. In this work, the RH 70%, 80%, and 90% were utilized and the 400 ppm, 700 ppm, and 1200 ppm CO_2 concentrations were provided to obtain the electrical energy harvesting using the form-stable 1-TD and PEG composites during the light-on/-off process.

2.2 Thermal and form stabilities of PCM composites

Fig. 4a shows the UV-Vis peaks of pre-vitrimer and SMV with different thicknesses. It is obvious that all SMVs can transmit sunlight. As a result, the sunlight can pass through the SMV container and cause the phase transition process in the PCMs inside. The thermal stability is important for the supporting material to maintain an initial solid state without damage. The temperature sweep result is reported in **Fig. 4b**. Both storage modulus and loss modulus decreased rapidly when the temperature was over 65 °C and the maximum Tan Delta appeared at 70 °C. It indicated that the glass transition temperature (T_g) was close to 70 °C and the SMV became flexible above 70 °C. Therefore, the thermal reliability tests for the two kinds of supporting materials were conducted under the change of external temperature from 25 °C to 80 °C. After several thermal cycles, the SMV supporting material kept the initial shape successfully while the pre-vitrimer fractured on the surface as shown in **Fig. 4c**. It was illustrated that the SMV supporting material exhibited a great flexibility and thermal stability

to prevent the damage subjected to thermal cycles. To demonstrate the shape memory effect of the SMV sample, the rectangular-shaped specimen was put into the MTS chamber to undergo a hot programming process. The temperature of the MTS chamber was increased to 150 °C and was maintained to achieve a thermal equilibrium state. Then the specimen was compressed at a loading rate of 0.20 mm/min until 13% strain. The cooling and unloading process were followed to complete the whole compression programming process[44]. **Eqns. (1)** and **(2)** are used to calculate the shape fixity ratio R_f and shape recovery ratio R_r, respectively:

$$R_f = \frac{\varepsilon_f}{\varepsilon_l} \times 100\% \quad (1)$$

$$R_r = \frac{\varepsilon_l - \varepsilon_t(N)}{\varepsilon_l - \varepsilon_t(N-1)} \times 100\% \quad (2)$$

where ε_f is the fixed strain after removing the load and ε_l is the strain before load removal. The $\varepsilon_t(N)$ and $\varepsilon_t(N-1)$ are the final strains of the samples with shape memory effect above the glass transition temperature (T_g). For total recovery, $\varepsilon_t(N-1)$ is eliminated when the $N = 1$ ($\varepsilon_t(0)$ equals to 0)[45].

The results of shape fixity ratio R_f and shape recovery ratio R_r were listed in **Table 2**. The SMV showed excellent shape recovery property and it can contribute to keep the high thermal stability without damage. Based on the close-then-heal (CTH) strategy[46], recovery stress plays an important role in bringing fracture surfaces in touch. Therefore, a recovery stress test was conducted. The compression programmed SMV sample was placed back into the MTS chamber and started the recovery test. **Fig. 4d** shows the SMV recovery stress at 90 °C as a function with time. It was found that the maximum stress was 1.84 MPa, which is sufficient to close micro-scale fatigue cracks[47]. Therefore, the SMV can heal the potential fatigue cracks under cyclic thermal loading.

To confirm the form stability of the SMV supported PCM composites, optical images of the pure PCM and PCM composites were taken, which demonstrated the form stabilities, as shown

in **Fig. S11**. It indicates that both the pure 1-TD and PEG were fully melted into the liquid state at 80 °C. The different sizes of the SMV supported PCM composites maintained the initial solid state without any leakage during the melting process. The volume expansion results of the PCM composites are shown in **Fig. S12a** and **S12b**. The different sizes of the SMV containers merely exhibit a slight volume expansion especially for the 3.5 mm and 4.0 mm thick specimens. The thermal conductivity measurement was conducted and both the SMV supported 1-TD and PEG composites was close to 0.33 W/mK as indicated in **Fig. S12c**. Definitely, the thermal conductivity of the PCM composites were mainly correlated to the SMV container. **Fig. S12d** shows the XRD peaks of the SMV, pure PCMs, and PCM composites. Only intrinsic crystal peaks appear, which confirms that no chemical reaction occurred between the SMV and pure PCMs. To verify the temperature gradients during the light-on/-off process, the IR camera images were taken as shown in **Fig. 5**. The temperature of the SMV container was changed rapidly while the SMV supported 1-TD and PEG composites underwent almost isothermal phase transition. From **Fig. 5b** and **5c**, it is seen that the SMV supported PEG and 1-TD composites had nearly an isothermal process within a certain period of time (a section of the temperature-time curve is almost a horizonal line), which is the phase transition period of each PCM. It is also seen that the period of time corresponding to the isothermal process for these two composites is different, suggesting that a certain temperature gradient can be maintained to trigger the Seebeck effect. The DSC results of the SMV and pure PCMs demonstrated the phase change temperature and latent heat (ΔT) property, as shown in **Fig. S13**. The PEG had higher melting and cooling points (T_{mp}, T_{cp}) than those of 1-TD, as shown in **Fig. S13b**, and **S13c**. From **Fig. S13a**, it is seen that the SMV is also stable after 100 thermal cycles. The stability under thermal cycles of the SMV, 1-TD, and PEG can be further validated by **Fig. S13d**. Furthermore, the DSC cycling results are listed in **Table S2.** It is seen that there

is only a slight difference after completing the 100 heating/cooling cycles, suggesting that the composite assembly is stable.

The SMV supported PCM composites maintain excellent thermal and chemical stabilities during the cycling test, which is also validated by the XRD peaks as shown in **Fig. S13d**. Therefore, the SMV container can support the pure 1-TD and PEG to fabricate form-stable PCM composites, which can be further utilized in smart and controllable energy harvesting.

2.3 Electrical energy harvesting under different conditions

The sunlight intensity on the surface of the PCM composites was defined as 15 mW/cm^2 which exhibited an appropriate electrical energy harvesting during the light-on/-off process[48]. The final temperatures of the SMV with different RHs are shown in **Fig. S14a**. It is clear that the SMV can reach 81 °C within the range of RH from 40% to 90%. At the initial air condition with 400 ppm CO_2, the electrical resistivity of the SMV was gradually increased during the light-on heating process. The decrease in CO_2 dissolving ability caused the low ion concentration in the moisture at different RHs as shown in **Fig. S14b, S14c, and S14d**. However, after increasing the CO_2 concentration to 700 ppm, the electrical resistivity became lower than the initial state as shown in **Fig. S15a, S15b, and S15c**. At the highest CO_2 concentration up to 1200 ppm, the electrical resistivity was a little lower than that at the 700 ppm concentration level due to the dissolving of additional CO_2 as shown in **Fig. S15d, S15e, and S15f**. Thus, the 700 ppm and 1200 ppm CO_2 concentrations can provide a good external environment to make a conductible SMV structure. **Fig. S16** shows the electrical resistivity of the SMV supported 1-TD and PEG composites with different SMV container sizes at RH 70% condition. Both the SMV supported 1-TD and PEG composites merely exhibited a slight difference within the range of CO_2 concentration from initial 400 ppm to 1200 ppm. The electrical resistivity at the RH 80% and 90% is similar as shown in **Fig. S17 and Fig. S18**, respectively. However, the PCM has an optimum volume size in order to effectively transfer

the stored thermal energy to electrical energy during the phase transition process[49]. To find out the optimum size of the SMV supported PCM composites, the temperature variation test was conducted and **Fig. S19** shows the result of different sizes of the 1-TD composite under different CO_2 concentrations. It is clear that the 2.5 mm and 3.0 mm thick SMV container supported 1-TD composites exhibit a lower phase transition field. The 3.5 mm and 4.0 mm thick SMV supported 1-TD composites had a similar result under the 400 ppm, 700 ppm, and 1200 ppm CO_2 concentrations. On the other hand, the 3.5 mm thick SMV supported PEG composite exhibited the most appropriate temperature peaks as shown in **Fig. S20**. Based on the results of temperature peaks, the 3.5 mm thick SM supported 1-TD and PEG composites were selected to generate electrical energy under different RH and CO_2 concentrations.

Fig. S21 shows the temperature peaks of the 1-TD composite under the three different CO_2 concentrations during the light-on/-off process. The CO_2 concentration changes from the initial 400 ppm to 1200 ppm, the heating rate was increased under the light-on heating process while the cooling rate was decreased due to the CO_2 greenhouse effect. The PEG composite saw the same effect as the 1-TD composite at the same range of RH and CO_2 concentrations, as shown in **Fig. S22**.

To observe the electrical energy output during the light-on/-off process, different CO_2 concentrations were utilized at the initial RH 40%. No voltage and current were produced as presented in **Fig. S23**. The change of the RH on one side, as shown in **Fig. S24 and Fig. S25** during the light-on/-off process, merely illustrated the noise effect. Based on the above test, the RH at each side of the PCM composite assembly should be over 70 % to decrease the electrical resistivity of the SMV structure. Therefore, RH 70% was used on the 1-TD composite side and RH 80% was used on the PEG composite side to generate electrical energy. The results are shown in **Fig. S26**. Both the output voltage and current at the initial 400 ppm were lower than 700 ppm and 1200 ppm CO_2 concentrations during the light-on/-off process. The first cycle of

voltage and current appeared up to 2300 s due to the temperature difference between the 1-TD and PEG composites. After the 1-TD composite completed the phase transition process, the temperature profile was reversed when the PEG composite underwent the phase transition field. The second peak lasted to 3500 s and the output current was lower than the 1st cycle because the high temperature decreased the CO_2 dissolving ability. On the contrary, the output voltage and current were produced rapidly due to the natural cooling during the light-off process. The 1st cycle was terminated at 1500 s and the energy harvesting maintained over 2500 s under the 700 ppm and 1200 ppm CO_2 concentrations. Compared with the light-on process, the 2nd cycle current peaks during the light-off process were higher because the CO_2 dissolving ability was increased under cooling. The output current was a little shifted due to the change of electrical resistivity under the change of external temperature. The maximum voltage and current were approximately 2.54 mV and 477.83 nA, respectively. Furthermore, the long-term durability test was conducted to demonstrate the repeatability under the 700 ppm and 1200 ppm CO_2 concentrations as shown in **Fig. S27** and **Fig. S28**, respectively. The second assembly was prepared using RH 80% 1-TD composite and RH 70% PEG composite. **Fig. S29** shows the results of voltage and current output during the light-on/-off process and the cycling results of energy harvesting are presented in **Fig. S30** and **Fig. S31**. The maximum voltage and current were close to 2.30 mV and 450.80 nA, which were lower than the first assembly. Basically, the PEG composite acted as the hot side of the PCM device due to the higher phase transition temperature than the 1-TD composite. It indicated that the high concentration of CO_2 at the hot side of the PCM device can increase the power output during the light-on/-off process. When the RH was over 80%, **Fig. S32, Fig. S33, and Fig. S34** show the assembly made of RH 80% 1-TD composite and RH 90% PEG composite. The high RH led to a decrease in the electrical resistivity, although the voltage and current outputs were even lower than the second assembly. The maximum voltage was close to 2.10 mV and the current was 443.00 nA at the high RH

condition. The RH 90% 1-TD composite and RH 80% PEG composite assembly was selected to generate electrical energy and the results are shown in **Fig. S35**. **Fig. S36** and **Fig. S37** exhibit the repeatable energy harvesting. The maximum voltage was 2.03 mV with 418.70 nA current output which exhibited lower efficiency for energy harvesting. Therefore, the concept of the Seebeck effect for energy harvesting requires the appropriate difference in electrical resistivity between the two sides of the materials. High RH with low electrical resistivity led to relatively low difference in electrical resistivity between 1-TD and PEG composites. As a result, increasing the difference between electrical resistivity was a key factor to improve the energy harvesting efficiency. Based on the above test results, RH 70% 1-TD composite with RH 90% PEG composite was utilized to observe the voltage and current output, and the results are shown in **Fig. 6**. It is easy to find out that the voltage and current outputs were higher than the previous assembly and the maximum voltage and current were 2.73 mV and 500.00 nA, respectively. **Fig. S38** and **Fig. S39** show the stable long-term durability during the phase transition process. Even with the change in RH between the 1-TD and PEG composites, the maximum voltage was close to 2.61 mV and the current was 474.60 nA as presented in **Fig. S40**, **Fig. S41**, and **Fig. S42**. Based on the output power test, the optimum external condition was defined as an assembly made of RH 70% 1-TD composite connected with RH 90% PEG composite.

2.4 Energy harvesting results by comparing with numerical simulations

To find out the maximum voltage and current outputs during the light-on/-off process, **Fig. 7** shows the results of the PCM composites with different RHs under the change of CO_2 concentrations. Based on the maximum voltage and current of 2.73 mV and 500.00 nA during the light-on process, the maximum outputs were 2.72 mV and 485.69 nA during the light-off process, which were higher than the previous research using the similar concept[50]. It demonstrated that the assembly with RH 70% 1-TD composite and RH 90% PEG composite

exhibited excellent electrical energy harvesting ability under the 700 ppm and 1200 ppm CO_2 concentrations during the light-on/-off process. To obtain the temperature profiles under the 700 ppm and 1200 ppm CO_2 concentrations, **Fig. S43** shows the results of the temperature curves during the light-on/-off process. The rate of temperature change was increased at the 1200 ppm level in **Fig. S43a** while the opposite result during the light-off process as shown in **Fig. S43b**. The output voltage was correlated to the temperature difference between the two sides of the PCM composites. **Fig. S44a and S44b** show the comparison between the measured temperature and the simulated result. It is clear that the numerical profiles have an agreement with the experimental peaks, which means the experimental results were correct during the light-on/-off process. **Fig. 8** shows the results of the voltage and current at 700 ppm and 1200 ppm by comparing with the numerical simulations. The maximum voltage and current were identical and the assembly made of RH 70% 1-TD composite and RH 90% PEG composite produced the electrical energy harvesting effectively. **Fig. S44c and S44d** show the comparison between the experimental and numerical peaks. There are no obvious differences at the 700 ppm and 1200 ppm CO_2 concentrations during the light-off process. In addition, the experimental voltage and current peaks were quite in agreement with the numerical simulation results as shown in **Fig. 9**, which demonstrates that the SMV supported PCM composites can generate stable and continuous electrical energy during the light-on/-off process. The electrical energy harvesting efficiency is presented in **Fig. S44e** and the light-on heating and light-off cooling efficiencies were approximately 61.88 % and 49.76 %, respectively, at the 700 ppm CO_2 concentration. Furthermore, the PCM composites under the 1200 ppm CO_2 concentration showed 61.76 % and 49.14 % efficiencies during the light-on/-off process. To summarize the experimental and numerical results, high RH with 700 ppm and 1200 ppm CO_2 concentrations can produce the electrical resistivity difference and harvest electrical energy during the PCM phase transition process.

3. Conclusions

In this work, we successfully synthesized a shape memory vitrimer (SMV) and 3D printed SMV hollow containers as a supporting material for the preparation of form-stable phase change material (PCM) composite. Both 1-tetradecanol (1-TD) and polyethylene glycol (PEG) infiltrated SMV containers exhibited excellent form-stability during the melting process of the PCMs without any leakage. The electrical energy harvesting was achieved by merely connecting the two different PCM composites. The energy harvesting efficiency was increased by changing the relative humidity (RH) and carbon dioxide (CO_2) concentrations on the surface of the SMV containers. This was an unprecedented discovery in the energy harvesting research area by using form-stable PCM composites during the light-on/-off process. It was found that high RH condition promoted the dissolving ability of CO_2, and the electrical resistivity was decreased significantly. Although the CO_2 dissolving ability changed under the temperature variation, the difference in electrical resistivity between the two sides of the PCM composite can induce the Seebeck effect and produce electrical energy during the light-on/-off process. It was found that the power output was decreased under high RH and high CO_2 concentration due to the similar electrical resistivity on the two sides of the composites. To overcome this problem, the assembly made of RH 70% 1-TD and RH 90% PEG composites were employed and obtained the highest voltage and current outputs up to 2.73 mV and 500 nA, respectively. The PCM composites showed high energy harvesting efficiency at 700 ppm and 1200 ppm CO_2 concentrations which indicated the greenhouse gas can be utilized to help harvesting energy. It has a high potential application in industry, vehicle, aerospace, household, and agriculture to produce a large amount of electrical energy from solar simply and easily.

It is noted that the use of CO_2 is to demonstrate that the greenhouse gas can be utilized to do something good. The concept proposed in this study, however, is general. Other organic or

inorganic compounds, be them solids, liquids, or gases, can also be employed as long as they can be dissolved into water to produce ions.

4. Experimental section

4.1 Materials

Diphenyl carbonate, Di(trimethylolpropane), Tris(2-aminoethylamine), Dichloromethane, Tris((2-(acryloyloxy)ethyl) isocyanurate (TAI), Diphenyl(2,4,6-trimethylbenzoyl)phosphine oxide (TPO), 1-tetradecanol (1-TD), and Polyethylene glycol (PEG, Mn= 6000) were purchased from the Sigma-Aldrich.

4.2 Preparation of shape memory vitrimer supporting material

The first step to fabricate a shape memory vitrimer (SMV) supporting material was to mix 90.0 g diphenyl carbonate with 21.0 g di(trimethylopropane) in a 140 °C oil bath for 2 hours. After that, 0.6 g tris(2-aminoethylamine) was dissolved in 6.50 mL dichloromethane (CH_2Cl_2), and was poured into the melted mixture which acted as a cross-linking agent to cause polymerization reaction as shown in **Fig. S2**. The pre-polymer was added to tris((2-(acryloyloxy)ethyl) isocyanurate (TAI) at a 120 : 90 mass ratio and stirred for 5 minutes. 9.0 g photo-initiator diphenyl(2,4,6-trimethylbenzoly)phosphine oxide (TPO) was then added to the polymer mixture. After that, the mixture was put into an oven at 120 °C for 30 minutes. The melted solution was then taken out and stirred for 1 hour with a stirring bar (500 rpm) and cooled down to room temperature in 30 minutes. As shown in **Fig. S3**, the pre-polymer was put into the 3D printer. The SMV hollow box with a dimension of 20 mm × 20 mm × 2.5 mm was printed by the 3D printer. To compare the mechanical and hydrophilic properties of the synthesized SMV, hollow box container was also printed by using TAI only, which was labeled as pre-vitrimer. To confirm the optimum thickness of SMV containers, four different container thicknesses were fabricated and labeled as 2.5 mm, 3.0 mm, 3.5 mm, and 4.0 mm.

4.3 Preparation of SMV supported form-stable PCM composites

Fig. S4a shows the fabrication route of form-stable PCM composite. The 3D printed SMV container has a 1 mm edge thickness which can prevent the pure PCM from leaking. The pure 1-TD and PEG were melted to a liquid state and poured into two SMV containers until full. The pre-polymer (pre-SMV) was painted onto two surfaces of the SMV containers and push them in contact. The assembly was then put into an ultraviolet (UV) chamber. After 80 seconds of UV curing treatment, a form-stable SMV supported PCM composite device was fabricated successfully. To determine an appropriate size of PCM composite device, the SMV containers with four different sizes, as shown in **Fig. S4b**, were utilized to fabricate the SMV supported 1-TD and PEG composites. The weight of SMV container and PCM composites are listed in **Table S1**. To verify the electrical resistivity under the change of external relative humidity (RH) and carbon dioxide (CO_2) concentrations, the initial state of RH 40% with 400 ppm CO_2 was changed gradually by increasing both the RH and CO_2 concentration.

4.4 Characterization

Fourier transform infrared spectroscopy (FTIR, Spectrum Two, PerkinElmer, MA, USA) was utilized to observe the chemical functional groups of the monomers and final SMV. The surface structures of the SMV and phase change materials (PCMs) were obtained by Field emission scanning electron microscope (FE-SEM, Quanta 3d FEG Dual Beam, FEI, Hillsboro, USA) after platinum coating. The transmittance of SMVs with various thickness were measured using UV-vis-NIR spectrophotometer under the 190 ~ 1000 nm wavelength (UV-3600, Shimadzu, Kyoto, Japan). The typical crystal structures of the PCM composites were measured by X-ray diffraction (XRD, Panalytical Empyrean, Malvern, UK) at the range of 10 – 60° with a scan rate of 3° min^{-1}. The stress-strain and shape recovery behaviors of the SMV were determined by using the 2610 Universal Testing Machine (UTM, Norwood, MA, USA). The sample dimension for recovery stress was 10.34 mm × 9.24 mm × 4.70 mm. A thermal

gravimetric analyzer (TGA550, TA Instruments, DE, USA) was utilized to measure the thermal stabilities of SMV and pure PCMs. For the SMV supported form-stable PCM composites, a rheometer (HR30, TA Instruments, DE, USA) was used to observe the volume expansion under the temperature variation from 25 °C to the final 80 °C. To demonstrate the SMV structures which were synthesized by monomers, X-ray photoelectron spectroscopy (XPS, Scienta omicron, Uppsala, Sweden) and Raman spectroscopy (Renishaw Invia Raman Microscope, TX, USA) were used to confirm the intrinsic functional peaks. A contact angle analyzer (FTA1000, First Ten Angstroms, VA, USA) was utilized to obtain the hydrophilic ability of the SMV material. The thermal conductivities of the pure PCM and PCM composites were confirmed by the thermal conductivity analyzer (C-Therm TCi, C-Therm Technologies Ltd, NB, Canada). The phase transition temperature and latent heat (ΔT) were obtained using a differential scanning calorimetry (DSC4000, PerkinElmer, MA, USA) with the range of 0 °C to 90 °C at a scanning rate of 10 °C/min. The temperature gradients of the SMV supported PCM composites during the light-on/-off process were observed by an IR high-resolution thermal camera (B20, HIKMICRO, Hangzhou, China). The temperature change of the SMV supported PCM composites was measured by a functional multi-meter (UT61, Guangdong, China), and the electrical energy output was recorded by a source meter (SourceMeter2400, KEITHLEY, OR, USA).

CRediT authorship contribution statement

Chengbin Yu: Conceptualization; methodology; validation; investigation; writing–original draft preparation. John Konlan: validation. Guoqiang Li: Supervision; funding acquisition; writing-revision & editing. All authors have read and agreed to the published version of the manuscript.

Funding

This work is funded by the US National Science Foundation under Grant Number OIA-1946231 and the Louisiana Board of Regents for the Louisiana Materials Design Alliance (LAMDA), the US National Science Foundation under grant number 1736136, and the US National Science Foundation under grant number 2051050.

Conflicts of Interest

The authors declare that they have no known competing financial interests or personal relationships that could have appeared to influence the work reported in this paper.

Acknowledgements

The authors would like to thank the Advanced Manufacturing and Machining Facility (AMMF) at Louisiana State University for providing the facilities to cut our samples. The authors also would like to thank Professor Qinglin Wu in the School of Renewable Natural Resources at Louisiana State University AgCenter for assisting in testing the contact angle.

References

1. K. K. Kurramovich, A. A. Abro, A. I. Vaseer, S. U. Khan, S. R. Ali and M. Murshed, *Environmental Science and Pollution Research*, 2022, 1-20.
2. Y. Shang, L. Zhu, F. Qian and Y. Xie, *Renewable Energy*, 2023, **206**, 890-896.
3. R. R. Hernandez, A. Armstrong, J. Burney, G. Ryan, K. Moore-O'Leary, I. Diédhiou, S. M. Grodsky, L. Saul-Gershenz, R. Davis and J. Macknick, *Nature Sustainability*, 2019, **2**, 560-568.
4. X. Liu, Y. Yuan, J. Liu, B. Liu, X. Chen, J. Ding, X. Han, Y. Deng, C. Zhong and W. Hu, *Nature communications*, 2019, **10**, 4767.
5. D. Fernández-González, I. Ruiz-Bustinza, C. González-Gasca, J. P. Noval, J. Mochón-Castaños, J. Sancho-Gorostiaga and L. F. Verdeja, *Solar Energy*, 2018, **170**, 520-540.
6. T. Ding, Y. Zhou, W. L. Ong and G. W. Ho, *Materials Today*, 2020.
7. P. Denholm, *Technical Potential of Solar Water Heating to Reduce Fossil Fuel Use and Greenhouse Gas Emissions in the United States*, National Renewable Energy Lab.(NREL), Golden, CO (United States), 2007.
8. X. Jin, S. W. Leow, Y. Fang and L. H. Wong, *Journal of Materials Chemistry A*, 2023.
9. A. K. Hamzat, M. I. Omisanya, A. Z. Sahin, O. R. Oyetunji and N. A. Olaitan, *Energy Conversion and Management*, 2022, **266**, 115790.
10. X. Mu, J. Zhou, P. Wang, H. Chen, T. Yang, S. Chen, L. Miao and T. Mori, *Energy & Environmental Science*, 2022, **15**, 3388-3399.
11. N. Sommerfeldt and J. M. Pearce, *Applied Energy*, 2023, **336**, 120838.
12. C.-T. Hsu, G.-Y. Huang, H.-S. Chu, B. Yu and D.-J. Yao, *Applied energy*, 2011, **88**, 5173-5179.
13. Y. Gao, M. Zhang, Y. Cui, D. Bao, F. Xu, X. Shen, Y. Zhu and H. Wang, *Journal of Materials Chemistry A*, 2022, **10**, 10452-10465.
14. X. Zhang, B. C. Shiu, T.-T. Li, X. Liu, H.-T. Ren, Y. Wang, C.-W. Lou and J.-H. Lin, *Chemical Engineering Journal*, 2021, **426**, 131923.

15. D. Liu, C. Lei, K. Wu and Q. Fu, *ACS nano*, 2020, **14**, 15738-15747.
16. W. Zhang, R. Mazzarello, M. Wuttig and E. Ma, *Nature Reviews Materials*, 2019, **4**, 150-168.
17. Y. Zhang, J. Wang, J. Qiu, X. Jin, M. M. Umair, R. Lu, S. Zhang and B. Tang, *Applied energy*, 2019, **237**, 83-90.
18. R. Gulfam, P. Zhang and Z. Meng, *Applied Energy*, 2019, **238**, 582-611.
19. D.-c. Gao, Y. Sun, A. M. Fong and X. Gu, *Energy Storage Materials*, 2022.
20. B. Zivkovic and I. Fujii, *Solar energy*, 2001, **70**, 51-61.
21. C. Yu and Y. S. Song, *Composites Communications*, 2023, **40**, 101600.
22. C. Yu, J. R. Youn and Y. S. Song, *Macromolecular Research*, 2019, **27**, 606-613.
23. Y. Cao, Y. Meng, Y. Jiang, S. Qian, D. Fan, X. Zhou, Y. Qian, S. Lin, T. Qian and Q. Pan, *Chemical Engineering Journal*, 2022, 134549.
24. D. Ghosh, J. Ghose, P. Datta, P. Kumari and S. Paul, *Journal of Energy Storage*, 2022, **53**, 105179.
25. P. Yan, W. Fan, Y. Yang, H. Ding, A. Arshad and C. Wen, *Applied Energy*, 2022, **327**, 120064.
26. H. Guo, W. Jiao, H. Jin, Z. Yuan and X. He, *Advanced Functional Materials*, 2023, **33**, 2209345.
27. Y. Chang, X. Yao, Y. Chen and D. Zou, *Composites Part B: Engineering*, 2023, 110584.
28. C. Yu, J. R. Youn and Y. S. Song, *Fibers and Polymers*, 2020, **21**, 24-32.
29. L. Wang and D. Meng, *Applied Energy*, 2010, **87**, 2660-2665.
30. C. Yu and Y. S. Song, *Nanomaterials*, 2021, **11**, 2192.
31. M. Zhou, D. Xie, K. Zhou, K. Gong, L. Yin, X. Qian and C. Shi, *Solar Energy Materials and Solar Cells*, 2022, **236**, 111537.
32. C. Yu and Y. S. Song, *Journal of Energy Storage*, 2023, **58**, 106360.
33. C. Yu and Y. S. Song, *Energy Technology*, 2023, **11**, 2201108.
34. Z. Niu and W. Yuan, *ACS Sustainable Chemistry & Engineering*, 2019, **7**, 17523-17534.
35. C. Yu, J. R. Youn and Y. S. Song, *Macromolecular Research*, 2021, **29**, 534-542.
36. J. Konlan, P. Mensah, S. Ibekwe and G. Li, *Journal of Composite Materials*, 2022, **56**, 2267-2278.
37. F. Meng, M. O. Saed and E. M. Terentjev, *Nature Communications*, 2022, **13**, 5753.
38. G. Li and D. Nettles, *Polymer*, 2010, **51**, 755-762.
39. L. Lu, J. Pan and G. Li, *Journal of Materials Chemistry A*, 2017, **5**, 21505-21513.
40. X. Feng and G. Li, *ACS Applied Materials & Interfaces*, 2020, **12**, 57486-57496.
41. Z. Feng, W. Zhao, Z. Yang, Y. Deng, T. Yang and Y. Ni, *Journal of Materials Chemistry A*, 2022, **10**, 11524-11534.
42. L. Rezende Franco, A. L. Sehnem, A. M. Figueiredo Neto and K. Coutinho, *Journal of Chemical Theory and Computation*, 2021, **17**, 3539-3553.
43. N. Abas and N. Khan, *Journal of CO2 Utilization*, 2014, **8**, 39-48.
44. A. Li, J. Fan and G. Li, *Journal of Materials Chemistry A*, 2018, **6**, 11479-11487.
45. P. Utroša, O. C. Onder, E. Žagar, S. Kovačič and D. Pahovnik, *Macromolecules*, 2019, **52**, 9291-9298.
46. G. Li and N. Uppu, *Composites Science and Technology*, 2010, **70**, 1419-1427.
47. A. Shojaei, S. Sharafi and G. Li, *Mechanics of Materials*, 2015, **81**, 25-40.
48. C. Yu, H. Kim, J. R. Youn and Y. S. Song, *ACS Applied Energy Materials*, 2021.
49. C. Yu, S. H. Yang, S. Y. Pak, J. R. Youn and Y. S. Song, *Energy Conversion and Management*, 2018, **169**, 88-96.
50. C. Yu and G. Li, *Energy Conversion and Management*, 2024, **299**, 117851.

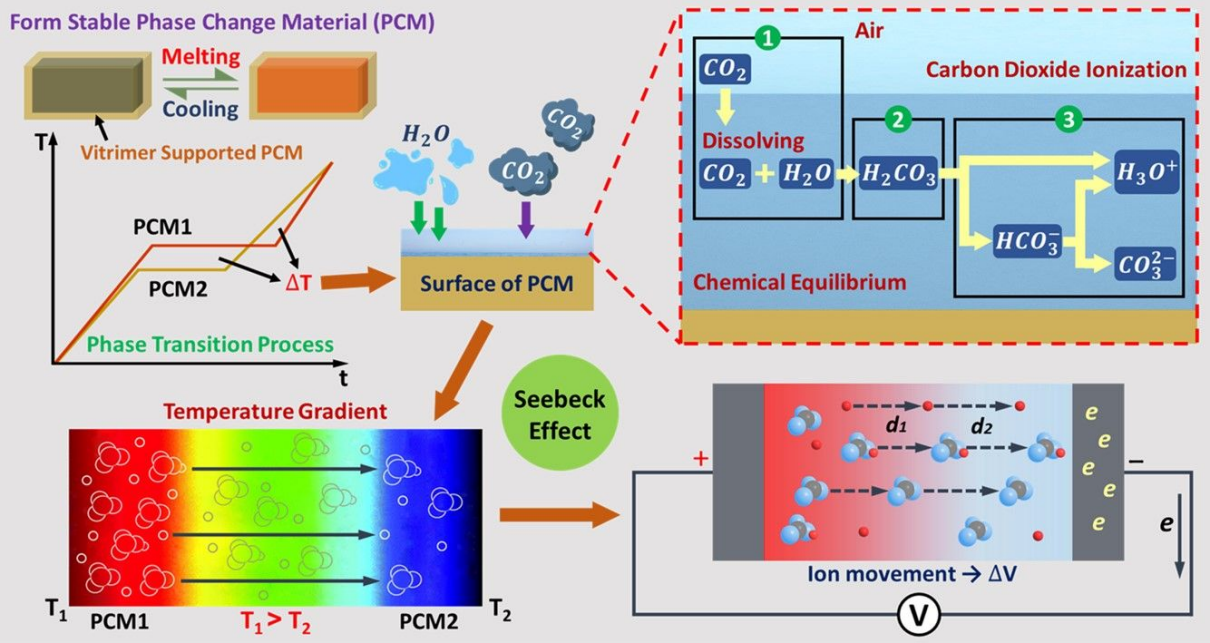

Fig. 1. Schematics of thermoelectric energy harvesting during the PCM phase transition process. The carbon dioxide (CO_2) can dissolve into the water to generate the hydrogen, bicarbonate, and carbonate ions to promote the electrical property. Definitely, the different CO_2 concentration occurs the various results of electrical energy harvesting during the light-on/-off process.

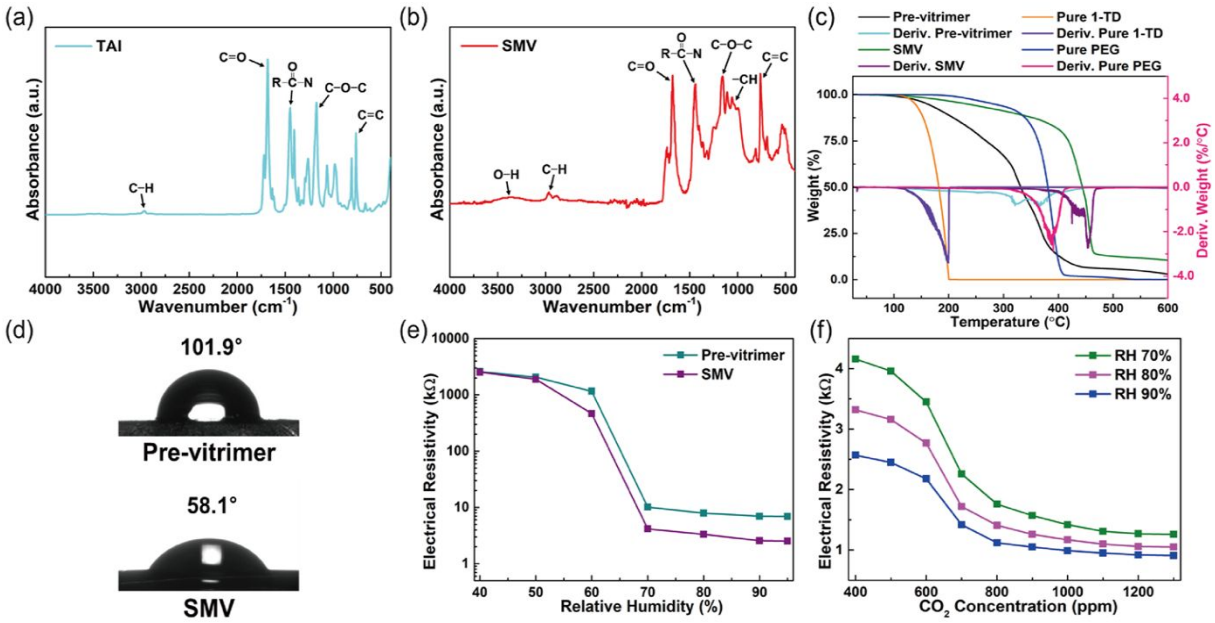

Fig. 2. FTIR results of (a) TAI and (b) final shape memory vitrimer (SMV). (c) TGA peaks of SMVs and pure PCMs. (d) contact angle results of pre-vitrimer and final SMV. (e) Electrical resistivity curves of pre-vitrimer and final SMV under the increase in RH at the initial CO_2 concentration. (f) Electrical resistivity peaks of SMVs at RH 70%, 80%, and 90% which are flexible under the change of CO_2 concentration.

Table 1. TGA data of Pre-vitrimer, SMV, and pure PCMs under N_2 atmosphere.

Samples	Onset (°C)	Peak (°C)	Endset (°C)	Residual mass (%)
Pre-vitrimer	**121.08**	**378.65**	**448.26**	**3.05**
SMV	**203.81**	**452.37**	**475.24**	**10.60**
Pure 1-TD	**148.40**	**191.52**	**202.03**	**0.06**
Pure PEG	**218.66**	**385.94**	**411.58**	**0.15**

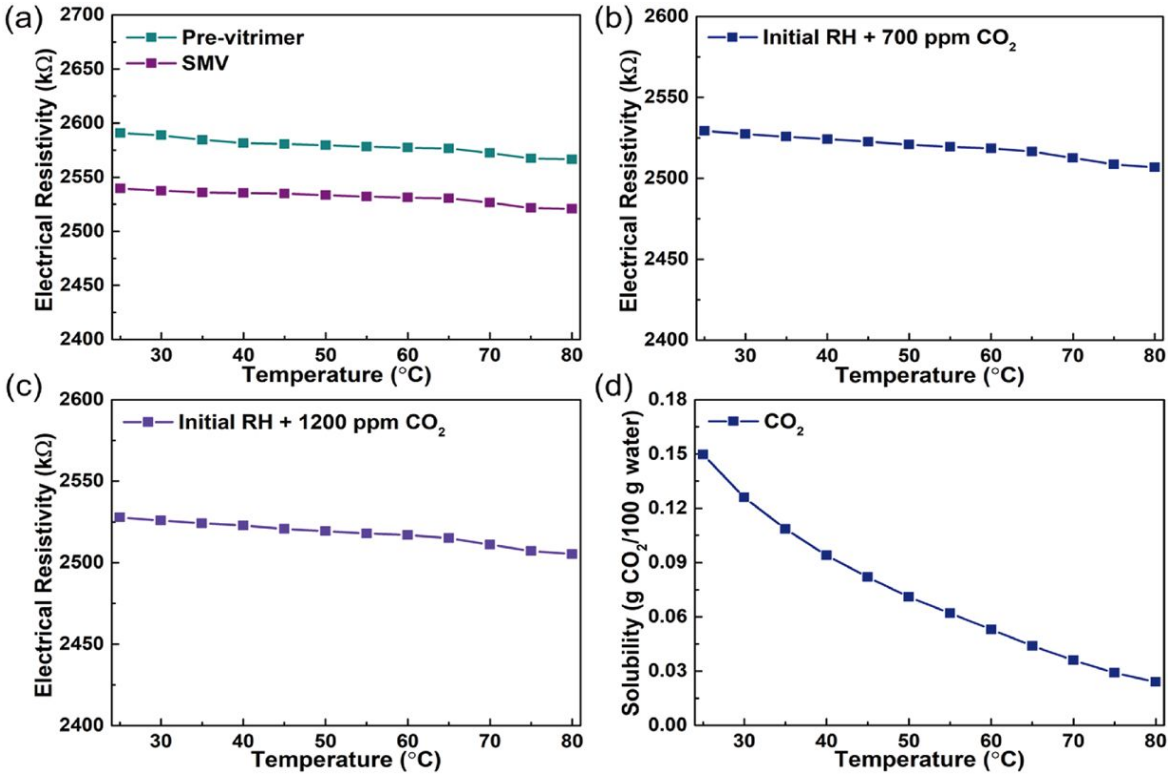

Fig. 3. Electrical resistivity of (a) pre-vitrimer and final SMV, (b) initial RH with 700 ppm CO_2 concentration, (c) initial RH with 1200 ppm CO_2 concentration, and (d) CO_2 dissolving ability under the temperature variation.

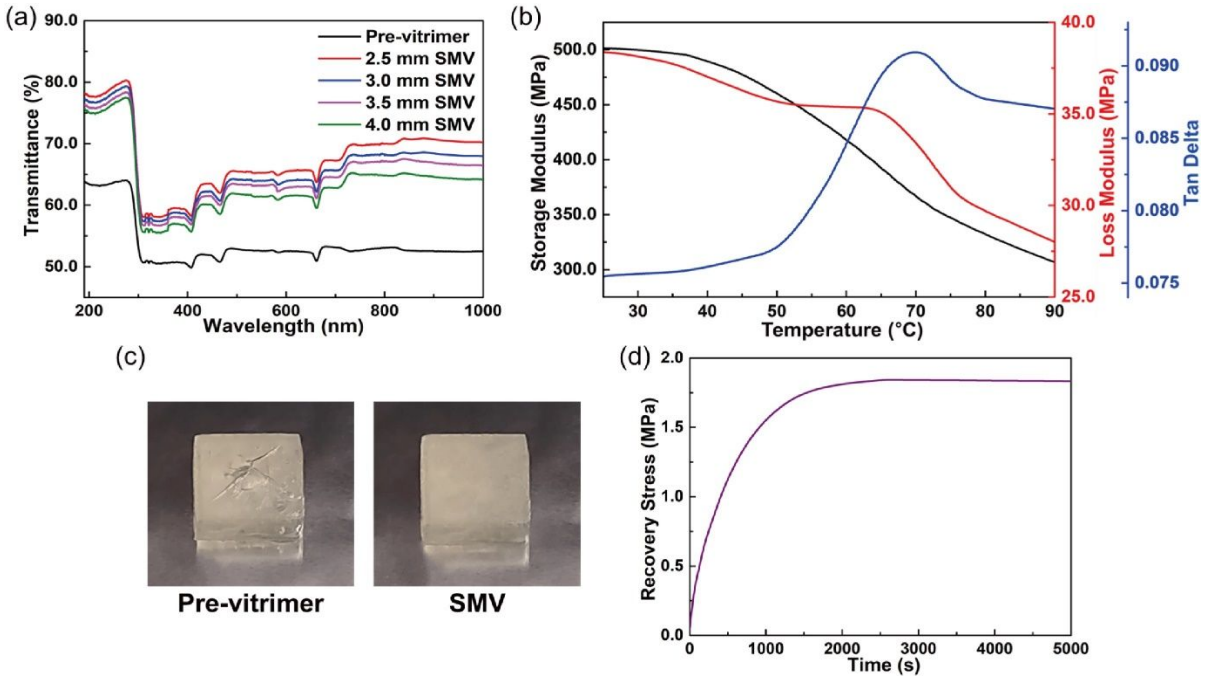

Fig. 4. (a) UV-Vis peaks of pre-vitrimer and SMV with different thickness. (b) Result of SMV temperature sweep. (c) Form stability photo images of pre-vitrimer and SMV after light-on/-off process. (d) Compressive stress of SMV at 90 °C. (e) Recovery stress of SMV at 90 °C.

Table 2. Shape fixity ratio (R_f) and shape recovery ratio (R_r) of the SMV.

Samples	Shape fixity ratio (R_f)	Shape recovery ratio (R_r)
Pre-vitrimer	**-**	**-**
SMV	**91.93%**	**99.00%**

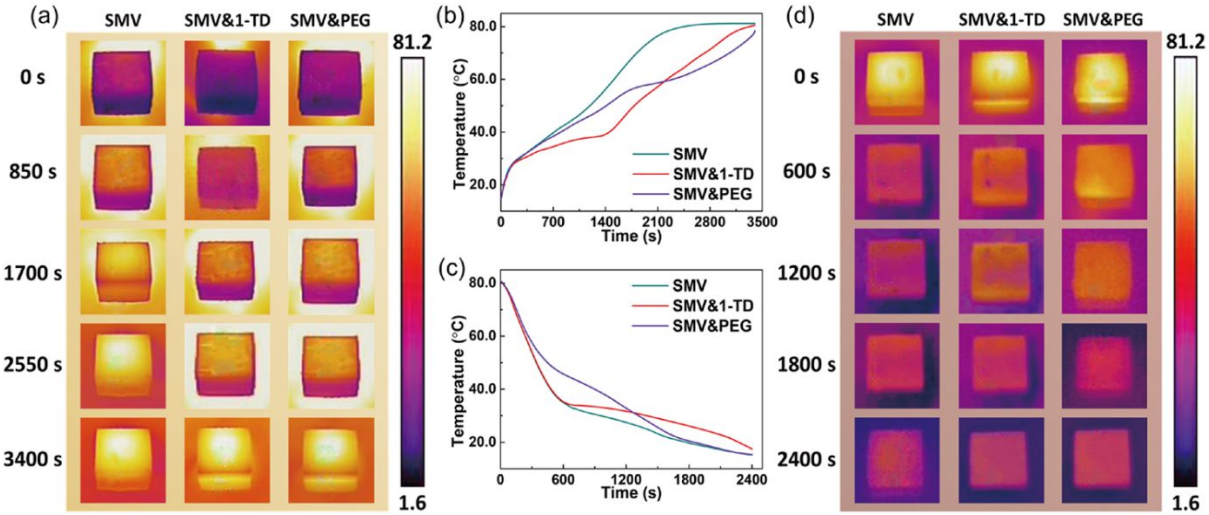

Fig. 5. (a) IR camera temperature gradient of SMV and SMV supported PCM composites during the light-on process. (b) Temperature peaks during light-on process. (c) Temperature peaks during light-off process. (d) IR camera temperature gradient of SMV and SMV supported PCM composites during the light-off process.

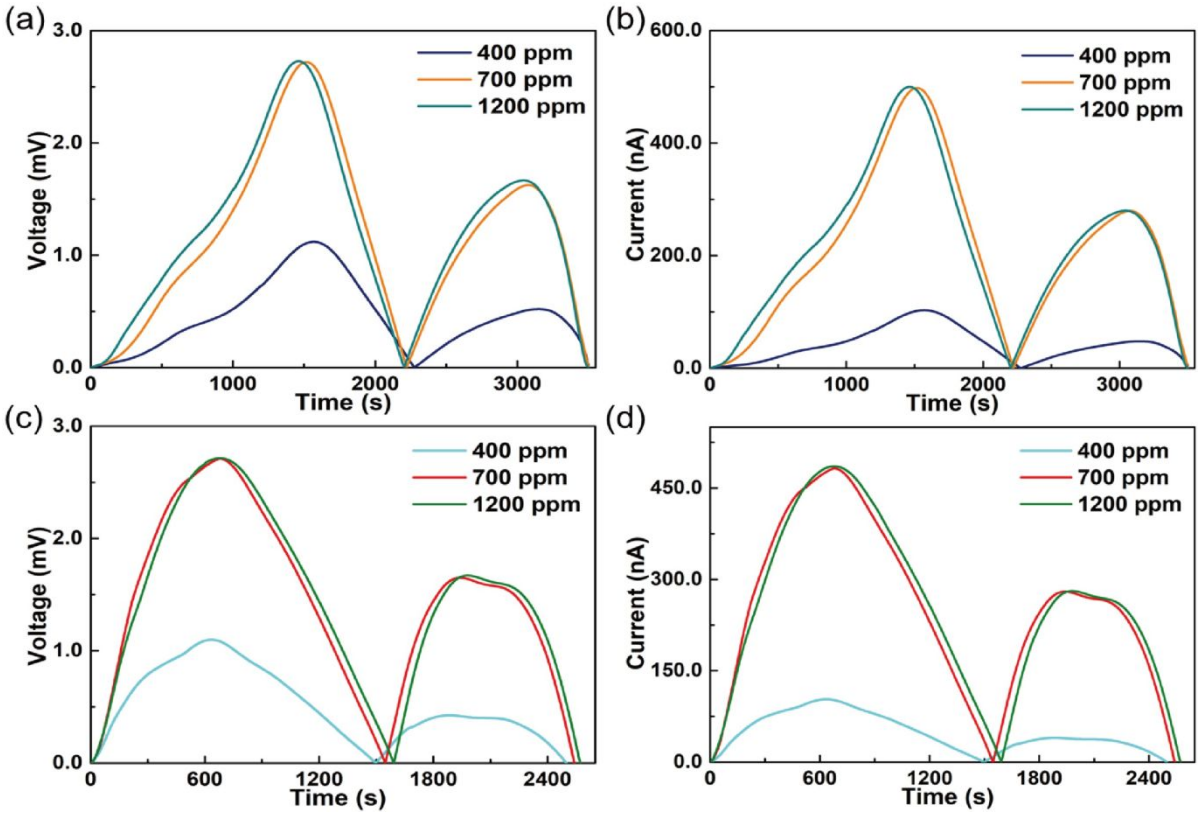

Fig. 6. For the assembly made of RH 70% SMV supported 1-TD and RH 90% SMV supported PEG, (a) output voltage with different CO_2 concentrations during the light-on process and (b) output current with different CO_2 concentrations during the light-on process. (c) Output voltage with different CO_2 concentrations during the light-off process and (d) output voltage with different CO_2 concentrations during the light-off process.

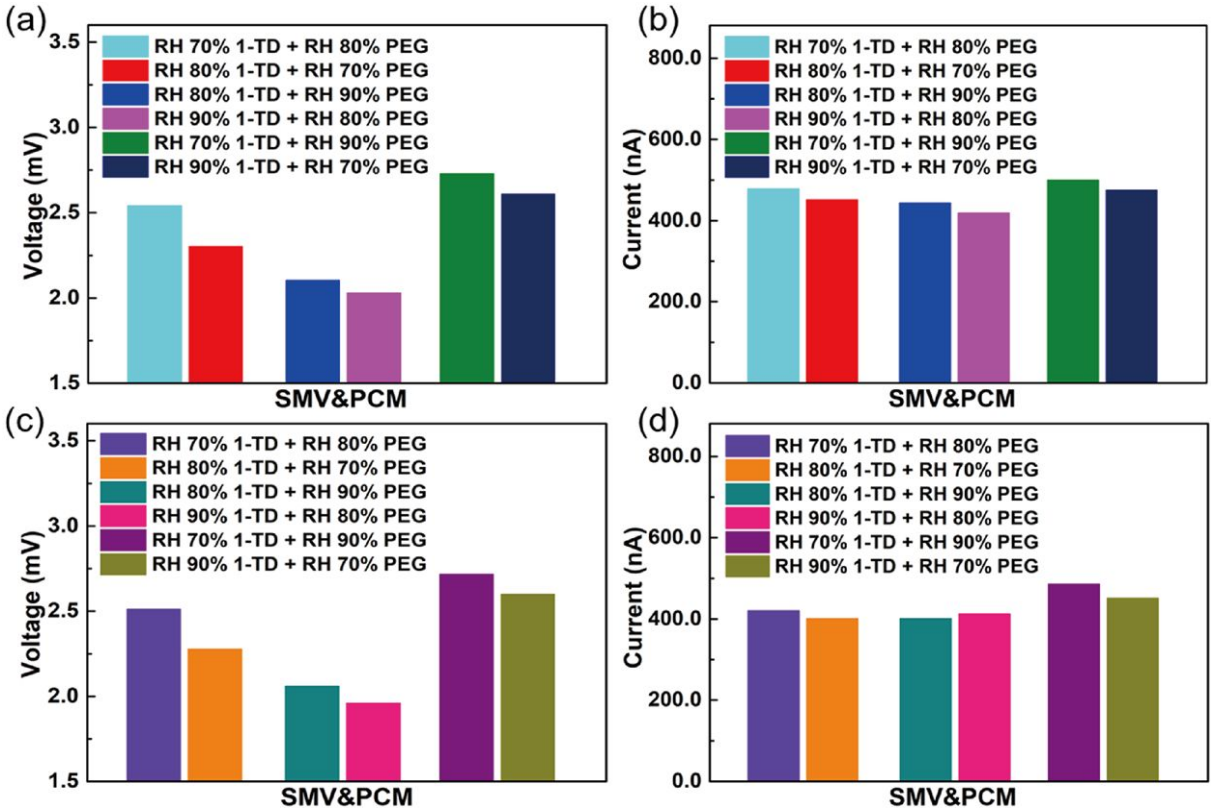

Fig. 7. For the light-on/-off process with different CO_2 concentration, (a) maximum output voltage under the light-on process and (b) maximum output current under the light-on process. (c) Maximum output voltage under the light-off process and (d) maximum output current under the light-off process.

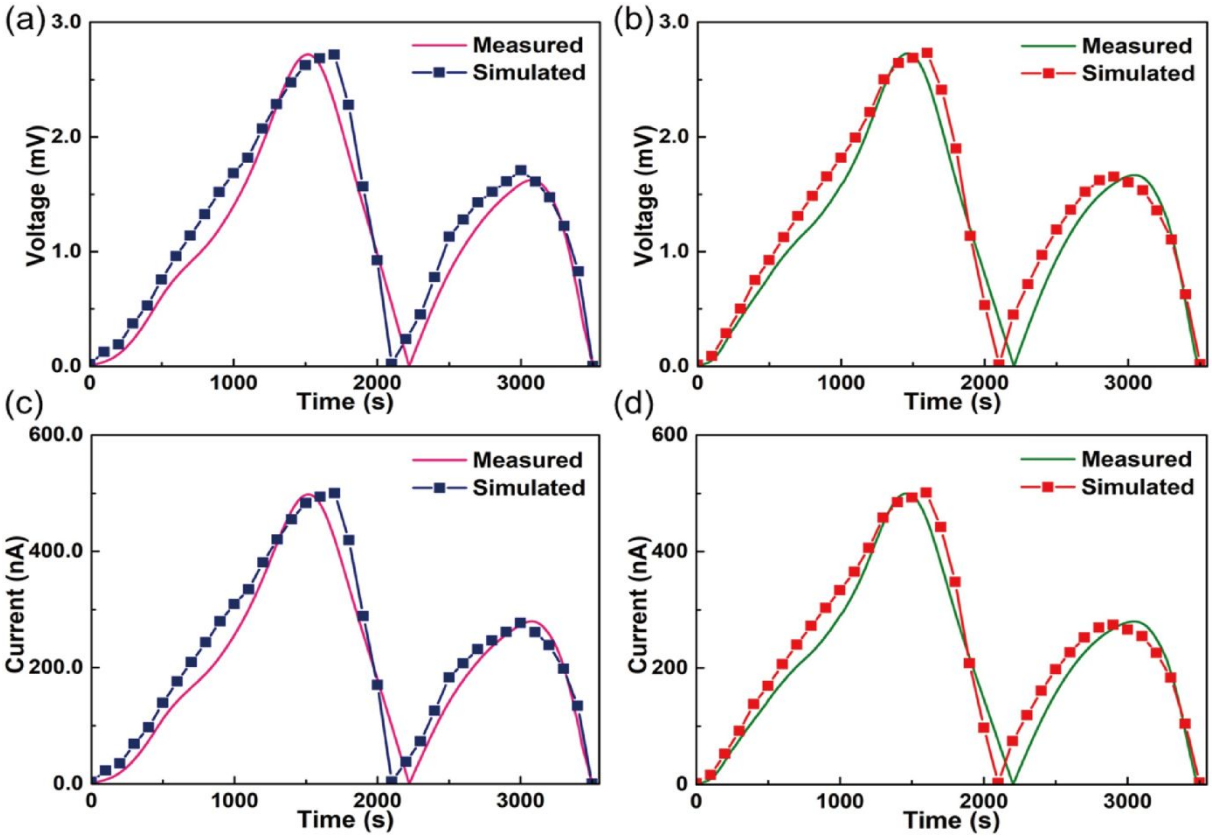

Fig. 8. For the assembly made of RH 70% SMV supported 1-TD and RH 90% SMV supported PEG, the comparison with simulated profiles upon light-on process, (a) output voltage under the 700 ppm CO_2 concentration and (b) output voltage under the 1200 ppm CO_2 concentration. (c) Output current under the 700 ppm CO_2 concentration and (d) output current under the 1200 ppm CO_2 concentration.

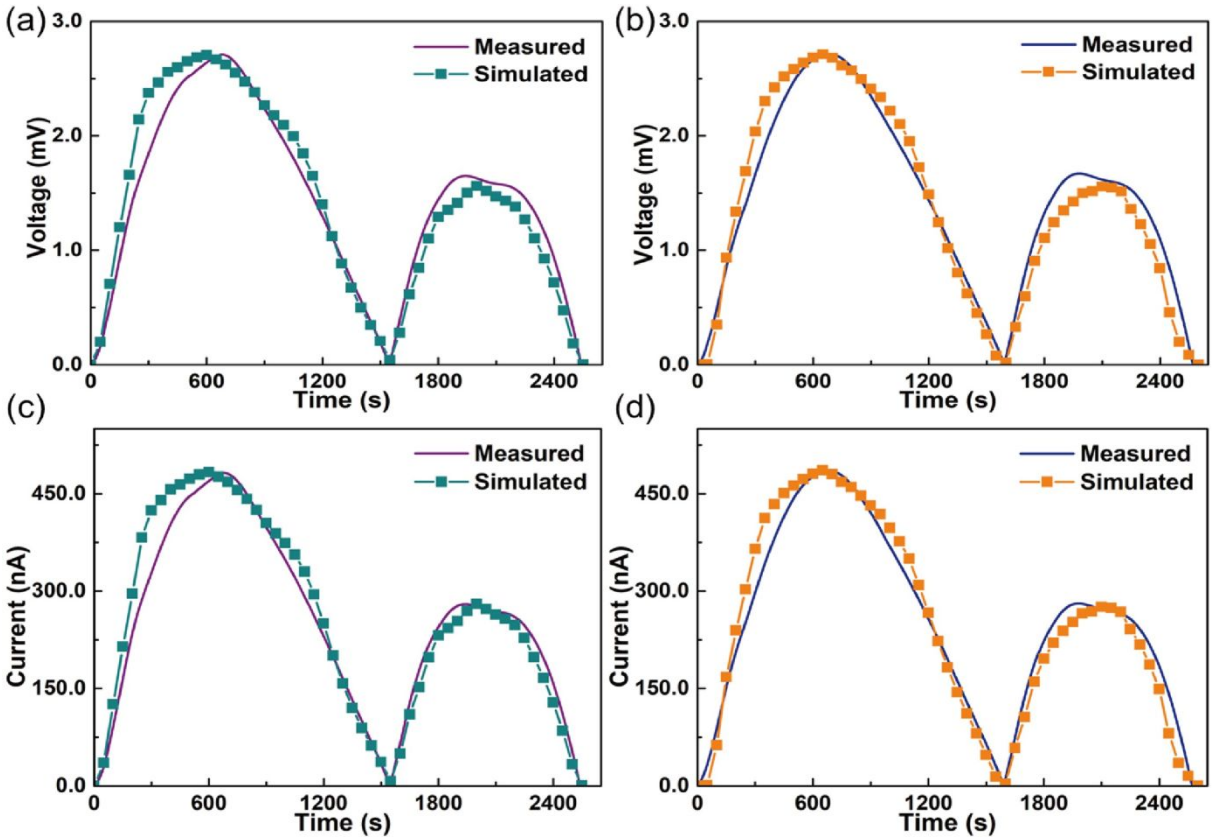

Fig. 9. For the assembly made of RH 70% SMV supported 1-TD and RH 90% SMV supported PEG, the comparison with simulated profiles upon light-off process, (a) output voltage under the 700 ppm CO_2 concentration and (b) output voltage under the 1200 ppm CO_2 concentration. (c) Output current under the 700 ppm CO_2 concentration and (d) output current under the 1200 ppm CO_2 concentration.